Int. J. Electrochem. Sci., 17 **(2022)** Article Number: 221235, doi: 10.20964/2022.12.29

International Journal of
ELECTROCHEMICAL
SCIENCE
www.electrochemsci.org

Comparative Analysis of Infrared and Electrochemical Fingerprints of *Magnolia officinalis* After Water Steam Treatment

Jing Xu[1], *Qinghua Gao*[2], *Wenliang Lv*[1,*]

[1] Clinical College of Chinese Medicine, Hubei University of Chinese Medicine, Wuhan 430000, Hubei Province, China
[2] College of Basic Medical Sciences, Hubei University of Chinese Medicine, Wuhan 430000, Hubei Province, China
[*]E-mail: lvwenliang66@126.com

Received: 17 September 2022 / *Accepted:* 28 October 2022 / *Published:* 30 November 2022

Magnolia officinalis is a herb of traditional Chinese medicine and its properties change with different treatments (called "sweating"). In this work, infrared spectra and electrochemical fingerprints of *Magnolia officinalis* were collected before and after treatment. Meanwhile, different sweating methods and sweating parameters on the quality of *Magnolia officinalis* were examined. The FTIR spectra were resolved differently for different samples after the second order derivative. The electrochemical fingerprinting was further modeled in this work. The developed discriminant analysis (DA) model allowed a rapid identification of different *Magnolia officinalis* simultaneously. The results show that the prediction accuracy of both the calibration and validation sets characterizing the performance of the optimal DA model is 100.0%.

Keywords: *Magnolia officinalis*; Electrochemical fingerprint; Infrared spectroscopy; Intelligent identification; Second derivative

1. INTRODUCTION

The dried bark, root bark and branch bark of *Magnolia officinalis* are important herbal medicine. However, direct administration of spicy and strong medicine can be irritating to the throat [1–3], thus this traditional herb is required to be treated (called "sweating") before it is used. The treatment is a key processing method that can accelerate the transformation of chemical components in the herb while promoting the rapid drying of *Magnolia officinalis*, which ensures the excellent quality of the herb [4–6]. Previous studies showed that *Magnolia officinalis* treatment can substantially increase the content of active ingredients, leachate and volatile oil. In addition, the color of *Magnolia officinalis* can be largely

changed after treatment [7]. Before treatment, the inner surface of the herb is yellow, while after treatment, it turns to purple-brown or dark purple-brown. Traditionally, *Magnolia officinalis* is treated until the inner epidermis of the herb is purple-brown, which is considered as the end criteria for primary processing, but the current research on *Magnolia officinalis* treatment mainly focuses on process optimization [8]. Moreover, the mechanism of this process is still not quite clear in terms of the effect on the properties, chemical composition, and pharmacological effects of the herbs.

The essence of the color change of herbs is a series of physicochemical reactions triggered by changes in the intrinsic chemical composition, such as enzymatic reactions, which can change the color of herbal appearance by catalyzing the conversion of substrates, thus producing colored products[9]. Enzymatic browning has been recognized to be an important factor leading to color changes in herbs such as chrysanthemum, honeysuckle and heliotrope during processing. The high temperature and high humidity environment during the treatment creates favorable conditions for enzyme activities in *Magnolia officinalis* cells while intensifying its tissue cell respiration [10–12].

Infrared spectroscopy (IR) refers to the absorption spectrum measured by irradiating a sample with a continuous wavelength of infrared light being the light source, which is generated by molecules undergoing a jump in vibrational energy levels, also known as vibrational spectroscopy [13,14]. Since the British scientist Herschel discovered infrared radiation in 1800, infrared technology has evolved over almost two centuries and has been applied in the field of drug analysis since the early 20th century. Infrared spectroscopy is a modern detection technique that can provide comprehensive information about a sample [15,16]. It is superior to conventional analysis with its fast detection speed, non-destructive sample, easy operation, high sensitivity, high accuracy and wide detection range, thus its application fields have constantly been expanded [17–19]. At present, infrared spectroscopy is an effective tool for the identification and analysis of Chinese herbal medicines, herbal concoctions and proprietary Chinese medicines. It is an important approach to study the composition, structure and content of chemical components of traditional Chinese medicine, and its application value recognized in both the quantitative examination and qualitative identification of traditional Chinese medicine [20]. The application of infrared spectroscopy for "rapid and non-destructive" testing of Chinese medicine reflects the intrinsic material basis of Chinese medicine, and also effectively controls the overall quality of Chinese medicine on a macro level [21].

Electrochemical fingerprinting is an emerging analytical technique that has been applied to botanical investigations in recent years [22–25]. Some of the research works suggested that this analytical technique could be used for herbal medicine analysis. In this work, infrared spectra and electrochemical fingerprints of *Magnolia officinalis* were collected before and after treatment, and in the meantime, the effect of different sweating methods and sweating parameters on the quality of *Magnolia officinalis* was examined.

2. EXPERIMENTAL

2.1. Sample collection and treatment.

A total of 10 samples were taken and treated with water steaming. The temperature was controlled at 25 ℃ and the relative humidity was controlled at 75% during the entire experiment.

The samples a to i were steamed in a steamer for 3, 6 and 9 min, respectively, and then samples a to c were stacked for 3 d, samples d to f for 6 d, and samples g to i for 9 d. Sample j was directly spread and dried as a negative controlled substance. Finally, a total of 60 samples were obtained.

2.2. Test sample preparation

Samples for magnolol and honokiol detection: 0.2 g of *Magnolia officinalis* sample powder (sieved by No.3) is weighed in a conical flask with stopper, and 25 mL of methanol was added. It was then well shaken, tightly stopped, and soaked for 24 h. Afterwards, it was filtered. 5 mL of filtrate was measured and put in a 25 mL flask. Methanol was added to the scale and shaken well. Methanol was added to make a solution containing 40 μg and 24 μg of magnolol and honokiol per 1 mL respectively, and then the samples were obtained.

Samples for FTIR and electrochemical fingerprints detection: The *Magnolia officinalis* samples were dried and crushed with a high-speed grinder and passed through 80 mesh sieve.

2.3. Electrochemical fingerprints collection

Shanghai T&H CHI760E electrochemical workstation was adopted to detect electrochemical fingerprints of samples. A three-electrode system was used to detect the electrochemical fingerprints of plants. Glassy carbon electrode, platinum wire electrode and Ag/AgCl electrode were adopted as working electrode, counter electrode and reference electrode, respectively. Differential pulse voltammetry was applied in scanning the samples. The electrolytes were 0.1 M phosphatic buffer solution.

2.4. FTIR fingerprints collection

An appropriate amount of *Magnolia officinalis* powder was placed on the diamond surface of the SMART ITR attachment and smoothed out, and the herb powder was pressed down and secured with the knob above the diamond. An FTIR spectrometer (Nicolet iS10 MX) was adopted to collect the data. The spectral range was 4000~525 cm^{-1} with 16 cumulative scans per spectrum. The spectral resolution was 4 cm^{-1}, and carbon dioxide and water vapor interferences were deducted in real time during the scanning process.

2.5 Discriminant analysis (DA)

For DA, it is usually necessary to divide the data into two sets, one of which is the training model data and the other is the validation model data. A model is fitted by training set data first and then the effect of the model is validated with the other data set. The good performance on the test set data indicates that the fitted model is good. This model can therefore be used to predict the category of the new data by predicting other "unclassified" data. No preprocessing (NP), multiplicative signal correction (MSC),

standard normal variate transformation (SNV), first derivative (FD), second derivative (SD), Savitzky-Golay smoothing (SGS) and Norris derivative smoothing (NDS) have been adopted for pre-treating the electrochemical data.

2.6 Magnolol and honokiol content determination

The sample powder was weighed 0.2 g and placed in a conical flask with stopper. 25 mL of methanol was added and soaked for 24 h. It was then filtered and 5 mL of the filtrate was measured. It was put in a 25 mL flask and methanol was added to the scale. The content of magnolol and honokiol was determined according to the Pharmacopoeia of the People's Republic of China, 2015 edition. Octadecylsilane bonded silica gel was adopted as filler. The mobile phase was methanol-water (78:22), and the detection wavelength was 294 nm. The theoretical plate number was calculated as the peak of magnolol at no less than 3800.

3. RESULTS AND DISCUSSION

Figure 1 shows the FTIR maps of ten samples. The absorption peaks were mainly distributed around 3369, 2929, 2159, 2031, 1974, 1620, 1407, 1018, 930, and 866 cm^{-1}. Specifically, the strong absorption peak corresponding to 3369 cm^{-1} is the intermolecular hydrogen bond O-H stretching vibration absorption peak; the peak near 2929 cm^{-1} is the C-H stretching vibration [26]; the absorption peak near 1620 cm^{-1} is a calcium oxalate C-O bond stretching vibration absorption peak [27]; the absorption peak near 1407 cm^{-1} corresponds to the C-H bending vibration.; the absorption peaks in the region of 1200-950 cm^{-1} are C-O vibration absorption peaks [28]; the absorption peaks below 950 cm^{-1} are for sugar isomeric absorption peaks. It can be found in Figure 1 that the FTIR spectra of the ten *Magnolia officinalis* samples were very similar in peak shape due to the similarity in composition and content of the chemical components, but significant differences exist in the location, absorption intensity and shape of some characteristic absorption peaks [29]. The absorption peak of sample e is red-shifted by 6 $cm^{-1}$and that of sample f is blue-shifted by 10 cm^{-1} around 3369 cm^{-1}. Both c and b are redshifted by 5 cm^{-1}, while both d and g are blue-shifted by 4 cm^{-1} [30]. The peak positions of c are 2935 cm^{-1} and 2026 cm^{-1}, around 2929 cm^{-1} and 2031 cm^{-1}, respectively, which are blue-shifted by 6 and red-shifted by 5 cm^{-1}compared to the other nine samples [31]. Around 1620 cm^{-1}, the absorption peaks of d, e, f and g are blue-shifted by 3, 4, 4 and 5 cm^{-1}, respectively, compared to the other samples [32]. Around 1407 cm^{-1}, the peak position of c is at 1415 cm^{-1}, which is 8 cm^{-1} blue-shifted from the other samples. The differences in the surface functional groups presented by FTIR represent the differences in the small molecules of samples produced under different treatment conditions. The electrochemical activity of the small molecules in plant tissues leads to the change of their electrochemical behavior with different treatments. These changes in behavior will be described in detail in the following sections.

The location and intensity of the absorption peaks in the range of 1620-930 cm^{-1} vary among the ten samples, indicating differences in their chemical composition and content [33]. The absorption peak

of C-O-C stretching vibration near 1018 cm^{-1} was adopted as the basis for determining the polysaccharide composition [34]. The figure presents that the positions of the absorption peaks of the ten samples at 1018 cm^{-1} are shifted only a little, but differences in their absorption intensities are significant [35].

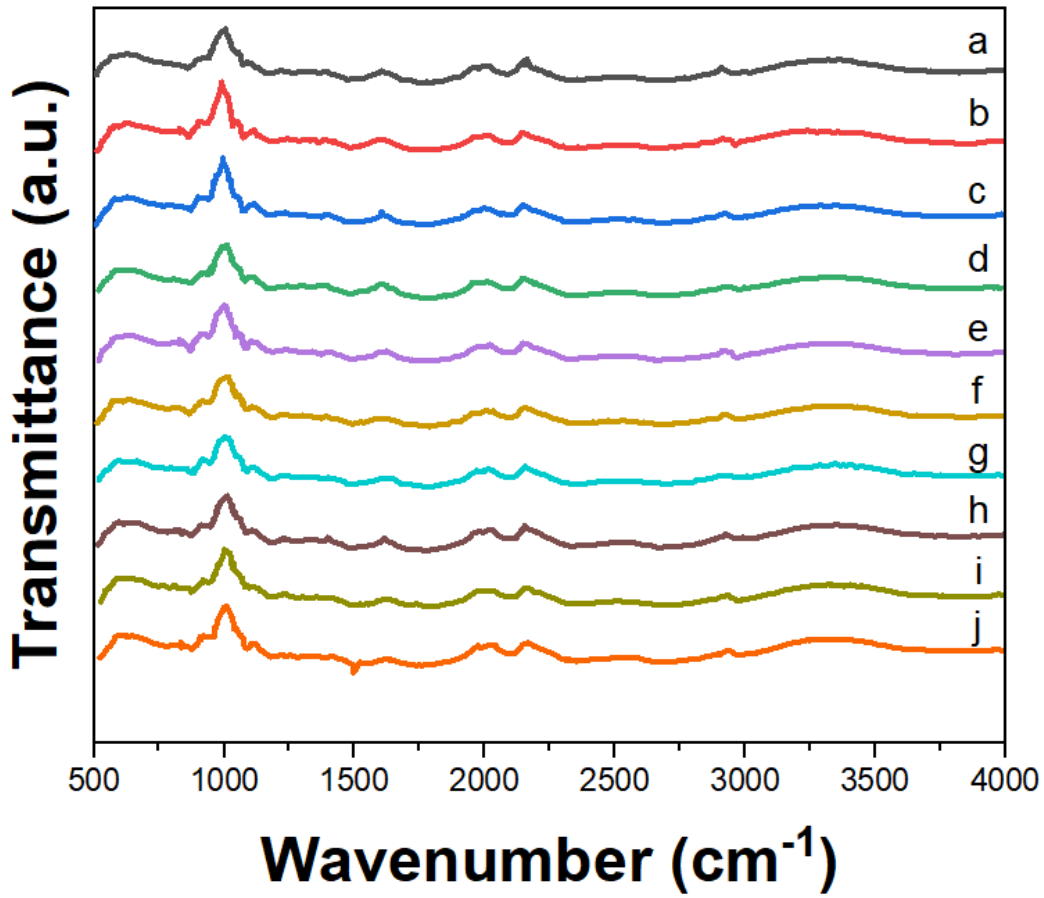

Figure 1. FTIR spectra of a-j samples of *Magnolia officinalis* recorded by mixing sample powder with the KBr.

Figure 2 shows the FTIR spectra of ten samples processed with second-order derivatives. The resolution is improved due to the stripping of overlapping peaks. Among the samples, the peak intensity of c is weaker in the range of 1700-1600 cm^{-1} compared with others, while f has the strongest characteristic absorption in this band [36]. In the region of 1600-1200 cm^{-1}, the strongest absorption peaks of a, b, d, and e are around 1507 cm^{-1}, while the strongest absorption of the other origins occurred around 1559 cm^{-1} [37]. The absorption peaks of all ten samples are near 1617 cm^{-1}, where the absorption intensities of c, e, i and j are relatively high, followed by the absorption intensities of d, e, h, and I, while b and j have the least intensities, indicating that there are differences in the calcium oxalate content of *Magnolia officinalis* from different origins [38]. In the range of 1200-980 cm^{-1}, the characteristic absorption peaks of sugar components are around 1018 cm^{-1} for all samples [39]. E, f, and h have the highest peak intensities, followed by a, c, and j, while b and i have the weakest intensities, further

verifying that the polysaccharide components of the ten samples are differentiated. All ten samples have the absorption peaks near 984 cm^{-1}, which correspond to steroidal saponin components [40]. However, significant difference exists in the locations and peak intensities of the absorption peaks. The second-order derivative spectra show that all ten *Magnolia officinalis* contain sugars, calcium oxalate and saponins, with different content. Compared with a normal FTIR spectrum, this spectrum allows for a clearer analysis of the subtle differences among origins.

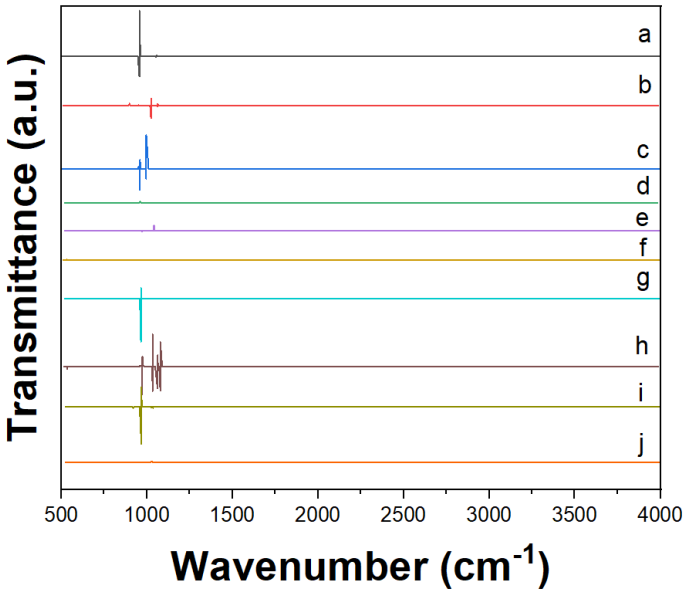

Figure 2. Second derivative FTIR spectra of a-j samples of *Magnolia officinalis* recorded by mixing sample powder with the KBr.

Figure 3 shows the electrochemical fingerprints of ten samples of *Magnolia officinalis*. It can be seen that *Magnolia officinalis* under different treatments show differences in the electrochemical fingerprints. It can be observed that these differences are larger than those in FTIR. A possible reason is that the different treatment times can result in some changes in the electrochemically active materials [41–43]. During the treatment process, some components that are originally electrochemically active are potentially oxidized, thus they lose the opportunity to participate in the electrochemical reaction. Samples a and c have larger oxidation peaks at 0.3 V, which probably represents higher flavonoid content in their tissues.

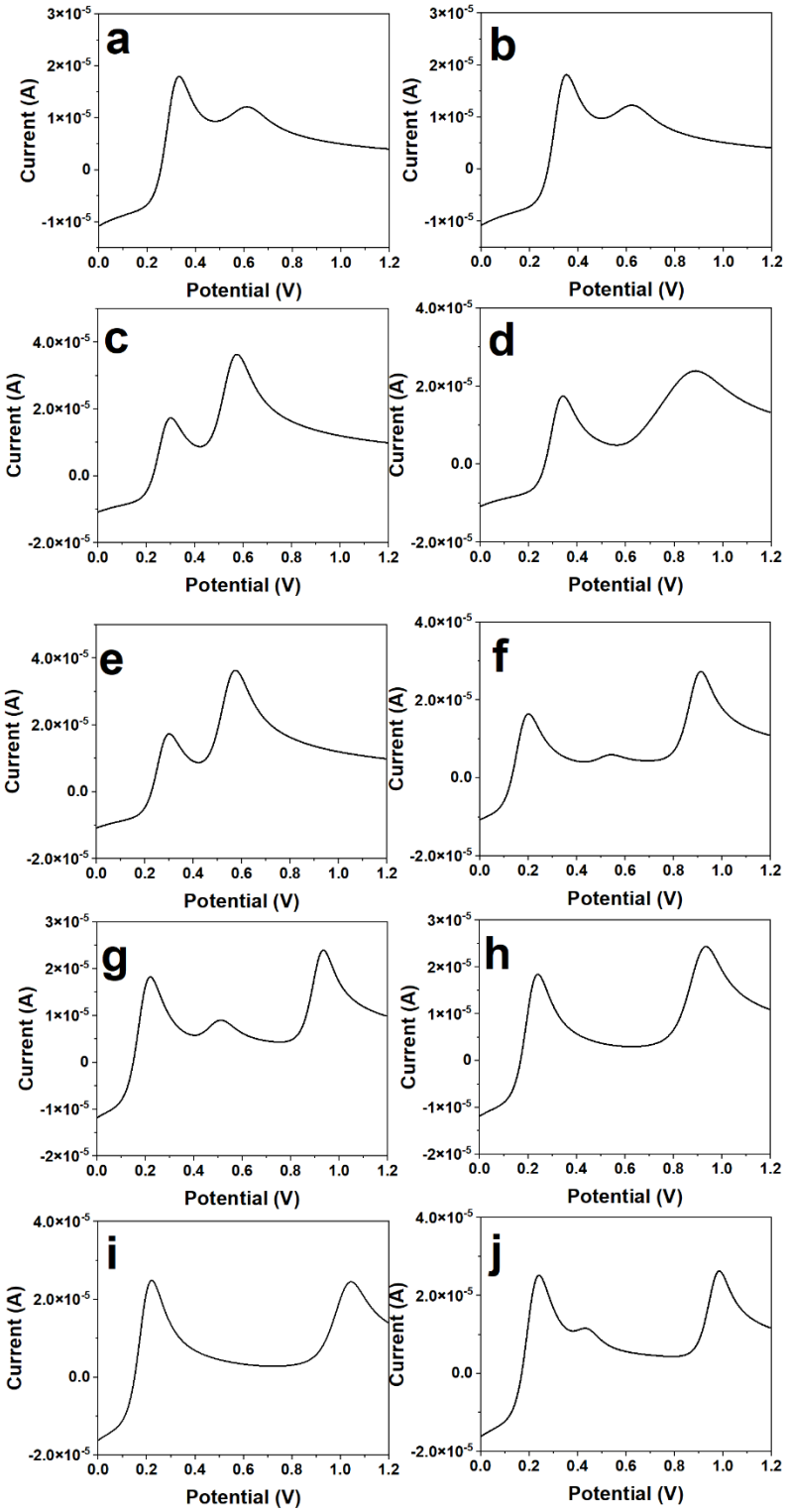

Figure 3. Electrochemical fingerprints of a-j samples of *Magnolia officinalis* under 0.1 M PBS.

In this study, further investigation were carried out by means of no preprocessing (NP), multiplicative signal correction (MSC), standard normal variate transformation (SNV), first derivative (FD), second derivative (SD), Savitzky-Golay smoothing (SGS), and Norris derivative smoothing (NDS)

in the pre-treatment method of electrochemical fingerprinting for reducing the interference and enhancing the sample signal [44,45]. As a result, the best performance of the discriminant analysis (DA) model was obtained for both MSC and SNV with TQ Analyst 8.0, as shown in Table 1. Therefore, MSC or SNV can be chosen for the pre-processing of electrochemical fingerprints [46].

After the electrochemical fingerprint data were processed by MSC, the modeled fingerprint profile range was selected within the scan range 0.2-0.7 V to improve model performance, simplify the model, and speed up the calculation. The results are shown in Table 1. The best modeling spectral range of 0.2-0.7 V for the DA model performance was obtained through the removal of the high noise part at both ends of the scan range, after which the results were manually selected. If a narrower potential range is applied, both the prediction accuracy of calibration and the prediction accuracy of validation of the DA model would be reduced.

Table 1. Main models and their performances of the DA

Model No.	Pre-treatment	Sub-range	Number of PCA	Prediction accuracy of calibration (%)	Prediction accuracy of validation (%)
1	NP	0.3-0.7 V	7	92.5	93.8
2	MSC	0.4-0.6 V	10	100	100
3	SNV	-	9	100	100
4	FD	-	7	95.4	92.4
5	SD	-	11	83.6	90.6
6	SGS	-	13	90.6	92.5
7	NDS	-	12	95.5	99.7
8	MSC+FD	-	10	93.2	96.1
9	MSC	0-1.2 V	10	91.8	92.4
10	MSC	0.3-0.7 V		96.6	93.5

To reduce data redundancy, TQ Analyst 8.0 was adopted to perform principal component analysis (PCA) dimensionality reduction on the electrochemical fingerprint data of three batches of samples. After the electrochemical fingerprint data were processed by MSC [47], the scores of the 3 PCs resulted in a highly overlapped sample distribution, which could not be identified. In this work, the DA was modeled with the scores of the top 10 PCs (with a cumulative contribution of 99.96%) and their reference values of the fingerprint data of the calibration set samples. It can be found in Figure 4 that the samples can be excellently identified.

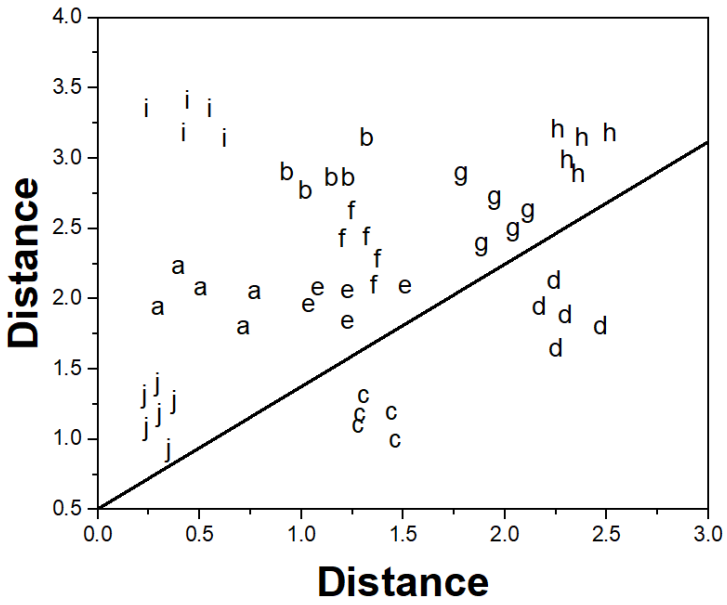

Figure 4. The DA discrimination of the samples of *Magnolia officinalis* with different treatments.

The changes of magnolol and honokiol content of the samples were analyzed in the same steaming time with the stacking time being the variable. The results of the average growth rate of magnolol and honokiol content are shown in Figure 5. The average growth rate of magnolol and honokiol content in *Magnolia officinalis* samples increases with the stacking time under the conditions of same steaming time[48,49]. The highest average growth rate of magnolol and honokiol content in *Magnolia officinalis* samples is achieved at the stacking time of g, h and i at 9 d. Statistical analysis shows that *Magnolia officinalis* samples have the highest increase in magnolol and honokiol content at 9 d of stacking time under the condition of same steaming time [50,51].

The changes of magnolol and honokiol content of the samples were analyzed in the same stacking time with steaming time being the variable. The average growth rate of magnolol and honokiol content under this condition are shown in Figure 6. The average growth rate of magnolol and honokiol content of *Magnolia officinalis* samples increases with the steaming time under the conditions of same stacking time [52]. The highest average growth rate of magnolol and honokiol content of *Magnolia officinalis* samples is achieved at the steaming time of c, f, and i. The highest increase in magnolol and honokiol content of *Magnolia officinalis* samples is at 9 min of steaming time under the condition of same stacking time [53,54]. The average growth rate of magnolol and honokiol content of the samples reaches the maximum value of 48. 51% at 9 min of steaming time and 9 d of stacking time.

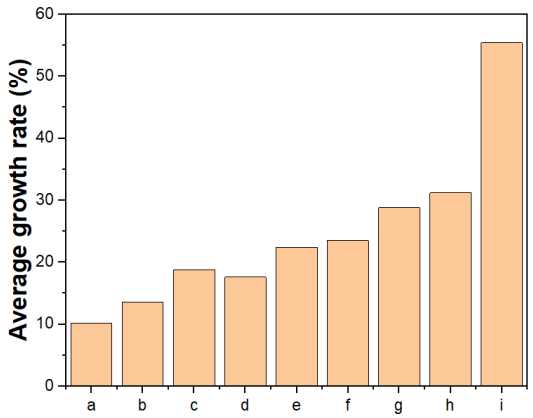

Figure 5. Average growth rate (%) of magnolol and honokiol content of *Magnolia officinalis* using different stacking time (a-c: 3 days; d-f: 6 days; g-i: 9 days).

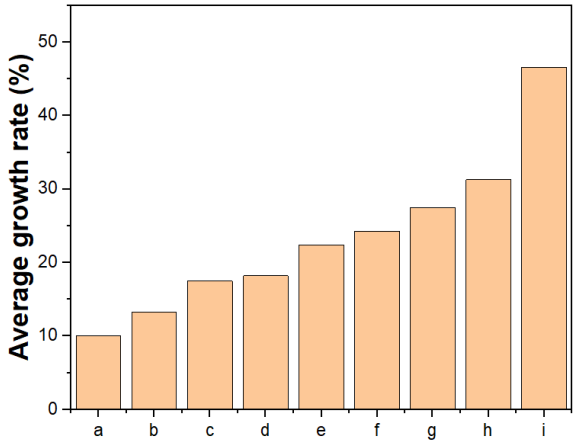

Figure 6. Average growth rate (%) of magnolol and honokiol content of *Magnolia officinalis* using different steaming time (a-c: 3 min; d-f: 6 min; g-i: 9min).

4. CONCLUSION

In conclusion, electrochemical and FTIR fingerprinting were adopted for the identification of *Magnolia officinalis* with different treatment methods in this work. The FTIR spectra were subjected to second-order derivatives to achieve differential resolution of different samples. The electrochemical fingerprinting was further modeled and the developed DA model allows a rapid identification of different *Magnolia officinalis* simultaneously. The result shows a 100.0% prediction accuracy of both the calibration and validation sets that characterize the performance of the optimal DA model. This work validates that electrochemical fingerprinting is a very promising way for the analysis of herbal medicines.

ACKNOWLEDGEMENTS
This work was financially supported by Local Cooperation Foundation of the Chinese Academy of Engineering from Hubei University of Chinese Medicine (No.3001-50150); Youth Project of Hubei University of Chinese Medicine (No.2022ZZXQ025).

References

1. V. Borgonetti, P. Governa, M. Biagi, N. Galeotti, *Nutrients*, 12 (2020) 1803.
2. Y.-H. Chen, M.-H. Lu, D.-S. Guo, Y.-Y. Zhai, D. Miao, J.-Y. Yue, C.-H. Yuan, M.-M. Zhao, D.-R. An, *Molecules*, 24 (2019) 2140.
3. K. Guo, C. Tong, Q. Fu, J. Xu, S. Shi, Y. Xiao, *J. Pharm. Biomed. Anal.*, 170 (2019) 153–160.
4. S. Khalid, A. Khan, B. Shal, H. Ali, Y.S. Kim, S. Khan, *Biomed. Pharmacother.*, 114 (2019) 108777.
5. C. Li, C.-J. Li, J. Ma, J.-W. Huang, X.-Y. Wang, X.-L. Wang, F. Ye, D.-M. Zhang, *Bioorganic Chem.*, 88 (2019) 102948.
6. C. Li, C.-J. Li, K.-L. Xu, J. Ma, J.-W. Huang, F. Ye, Y.-D. Zang, D.-M. Zhang, *Bioorganic Chem.*, 104 (2020) 104319.
7. L. Niu, Y. Hou, M. Jiang, G. Bai, *J. Ethnopharmacol.*, 281 (2021) 114524.
8. V.-T. Vu, X.-Q. Liu, M.-T. Nguyen, Y.-L. Lin, L.-Y. Kong, J.-G. Luo, *Bioorganic Chem.*, 96 (2020) 103586.
9. Z. Xue, C. Lai, L. Kang, A. Kotani, H. Hakamata, Z. Jing, H. Li, W. Wang, B. Yang, *J. Chromatogr. A*, 1611 (2020) 460583.
10. Y. Yin, F. Peng, L. Zhou, X. Yin, J. Chen, H. Zhong, F. Hou, X. Xie, L. Wang, X. Shi, B. Ren, J. Pei, C. Peng, J. Gao, *IScience*, 24 (2021) 102997.
11. Y. Yuan, X. Zhou, Y. Wang, Y. Wang, X. Teng, S. Wang, *Curr. Drug Targets*, 21 (2020) 559–572.
12. X. Zhi, L. Jiang, T. Li, L. Song, Y. Wang, H. Cao, C. Yang, *Bioorg. Med. Chem. Lett.*, 30 (2020) 127086.
13. M.A.F. Azlah, L.S. Chua, F.I. Abdullah, M.F. Yam, *Vib. Spectrosc.*, 106 (2020) 103014.
14. A. Brangule, R. Šukele, D. Bandere, *Front. Plant Sci.*, 11 (2020) 356.
15. K. Kucharska-Ambrożej, J. Karpinska, *Microchem. J.*, 153 (2020) 104278.
16. Y. He, M. Xu, L. Dong, J. Chen, *J. Mol. Struct.*, 1249 (2022) 131581.
17. N.K. Hemanth Kumar, J.D. Andia, S. Manjunatha, M. Murali, K.N. Amruthesh, S. Jagannath, *Biocatal. Agric. Biotechnol.*, 18 (2019) 101024.
18. R. Kaavya, R. Pandiselvam, M. Mohammed, R. Dakshayani, A. Kothakota, S. Ramesh, D. Cozzolino, C. Ashokkumar, *Appl. Spectrosc. Rev.*, 55 (2020) 593–611.
19. M.M. Oliveira, J. Cruz-Tirado, D.F. Barbin, *Compr. Rev. Food Sci. Food Saf.*, 18 (2019) 670–689.
20. A. Režan, M. Benković, T. Jurina, A.J. Tušek, J.G. Kljusurić, D. Valinger, *J. Hyg. Eng. Des.*, 27 (2019) 152–156.
21. G. Shi, B. Xu, X. Wang, Z. Xue, X. Shi, Y. Qiao, *J. Spectrosc.*, 2019 (2019) 4139762.
22. M. Chen, H. Yang, Z. Song, Y. Gu, Y. Zheng, J. Zhu, A. Wang, L. Fu, *Phyton-Int. Exp. Bot.*, 90 (2021) 1507–1518.
23. B. Fan, Q. Wang, W. Wu, Q. Zhou, D. Li, Z. Xu, L. Fu, J. Zhu, H. Karimi-Maleh, C.-T. Lin, *Biosensors*, 11 (2021) 155.
24. L. Fu, A. Yu, G. Lai, *Chemosensors*, 9 (2021) 282.
25. L. Fu, Y. Zheng, A. Wang, P. Zhang, S. Ding, W. Wu, Q. Zhou, F. Chen, S. Zhao, *J. Herb. Med.*, 30 (2021) 100512.
26. F. Wu, Y. Zhang, W. Liu, N. Zhu, J. Chen, Z. Sun, *J. Mol. Struct.*, 1204 (2020) 127554.

27. H. Issa-Issa, E. Ivanišová, L. Noguera-Artiaga, A. Kántor, D. López-Lluch, M. Kačániová, A. Szumny, Á.A. Carbonell-Barrachina, *Eur. Food Res. Technol.*, 245 (2019) 1197–1206.
28. J. Chen, J. Fan, D. Wang, S. Yue, X. Zhai, Y. Gong, J. Wang, *Spectrochim. Acta. A. Mol. Biomol. Spectrosc.*, 232 (2020) 118176.
29. S. Kasemsumran, W. Apiwatanapiwat, K. Ngowsuwan, S. Jungtheerapanich, *Chem. Pap.*, 75 (2021) 5633–5644.
30. A. Sharma, R. Chauhan, R. Kumar, P. Mankotia, R. Verma, V. Sharma, *Spectrochim. Acta. A. Mol. Biomol. Spectrosc.*, 258 (2021) 119803.
31. A.A. Bunaciu, H.Y. Aboul-Enein, *Appl. Spectrosc. Rev.*, 56 (2021) 423–437.
32. U. Sadowska, A. Matwijczuk, A. Niemczynowicz, T. Dróżdż, A. Żabiński, *Processes*, 7 (2019) 466.
33. C. Zhang, Z. Zhang, L. Zhang, H. Zhang, Y. Wang, S. Hu, J. Xiang, X. Hu, *Biomass Bioenergy*, 143 (2020) 105801.
34. Y. Li, Y. Shen, C. Yao, D. Guo, *J. Pharm. Biomed. Anal.*, 185 (2020) 113215.
35. M.M. Said, S. Gibbons, A. Moffat, M. Zloh, *J. Infrared Spectrosc.*, 27 (2019) 379–390.
36. A. Balkrishna, M. Tomer, S. Verma, M. Joshi, P. Sharma, J. Srivastava, A. Varshney, *J. Sep. Sci.*, 44 (2021) 4064–4081.
37. W. Pan, M. Wu, Z. Zheng, L. Guo, Z. Lin, B. Qiu, *J. Food Sci.*, 85 (2020) 2004–2009.
38. L. Yin, J. Zhou, D. Chen, T. Han, B. Zheng, A. Younis, Q. Shao, *Spectrochim. Acta. A. Mol. Biomol. Spectrosc.*, 221 (2019) 117208.
39. A.G. Osman, V. Raman, S. Haider, Z. Ali, A.G. Chittiboyina, I.A. Khan, *J. AOAC Int.*, 102 (2019) 376–385.
40. P. Li, Y. Zhang, Y. Ding, Q. Wu, Z. Liu, P. Zhao, G. Zhao, S. Ye, *Microchem. J.*, 181 (2022) 107767.
41. J. Zhou, Y. Zheng, J. Zhang, H. Karimi-Maleh, Y. Xu, Q. Zhou, L. Fu, W. Wu, *Anal. Lett.*, 53 (2020) 2517–2528.
42. Y. Zheng, X. Li, F. Han, L. Fu, J. Sun, *Int J Electrochem Sci*, 16 (2021) 211136.
43. W. Ye, Y. Zheng, P. Zhang, B. Fan, Y. Li, L. Fu, *Int J Electrochem Sci*, 16 (2021) 211041.
44. A. Dankowska, A. Majsnerowicz, W. Kowalewski, K. Włodarska, *Sustainability*, 14 (2022) 6416.
45. J.-E. Dong, Y. Wang, Z.-T. Zuo, Y.-Z. Wang, *Chemom. Intell. Lab. Syst.*, 197 (2020) 103913.
46. K. Kucharska-Ambrożej, J. Karpinska, *Microchem. J.*, 153 (2020) 104278.
47. W. Sohng, Y. Park, D. Jang, K. Cha, Y.M. Jung, H. Chung, *Talanta*, 212 (2020) 120748.
48. P. Chou, W. Chang, F. Liu, S. Lan, M. Sheu, J. Chen, *Food Sci. Nutr.*, 8 (2020) 1093–1103.
49. Y. Hu, Y. Shen, X. Tu, X. Wu, G.-X. Wang, F. Ling, *Bioorg. Med. Chem. Lett.*, 29 (2019) 389–395.
50. W. Jing, X. Zhao, M. Li, X. Hu, X. Cheng, S. Ma, F. Wei, *Molecules*, 27 (2022) 3892.
51. H. Kim, C.Y. Lim, M.S. Chung, *Foodborne Pathog. Dis.*, 18 (2021) 24–30.
52. H. Ni, X. Cai, X. Qiu, L. Liu, X. Ma, L. Wan, H. Ye, L. Chen, *Fitoterapia*, 147 (2020) 104769.
53. A. Vega-García, L. Rocha, R. Guevara-Guzmán, C. Guerra-Araiza, I. Feria-Romero, J.M. Gallardo, T. Neri-Gomez, J.E. Suárez-Santiago, S. Orozco-Suarez, *Curr. Pharm. Des.*, 26 (2020) 1388–1401.
54. J. Yang, Z.-X. Wang, L. Fang, T.-S. Li, Z.-H. Liu, Y. Pan, L.-D. Kong, *J. Ethnopharmacol.*, 300 (2023) 115688.